REFERENCES

Ashbaugh, H.S., Fetters, L.J., Adamson, D.H., and Prud'homme, R.K. (2002a) Flow improvement of waxy oils mediated by self-aggregating partially crystallizable diblock copolymers. Journal of Rheology, 46(4), 763-776.

Ashbaugh, H.S., Radulescu, A., Prud'homme, R.K., Schwahn, D., Richter, D., and Fetters, L.J. (2002b) Interaction of paraffin was gels with random crystalline/amorphous hydrocarbon copolymers. Macromolecules, 35(18), 7044-7053.

Beiny, D.H.M., and Mullin, J.W. (1987) Solubilities of higher normal alkanes in m-xylene. Journal of Chemical and Engineering Data, 32(1), 9-10.

Burgdorf, R., Zocholl, A., Arlt, W., and Knapp, H., (1999) Thermophysical properties of binary liquid mixtures of polyether and n-alkane at 298.15 and 323.15 K: heat of mixing, heat capacity, viscosity, density and thermal conductivity. Fluid Phase Equilibria, 164, 225-255.

Cermak, S.C., Brandon, K.B., and Isbell, T.A. (2006) Synthesis and physical properties of estolides from lesquerella and castor fatty acid esters Industrial Crops and Products, 23(1), 54-64.

Coutinho, J.A.P., and Daridon, J.-L. (2005) The limitations of the cloud point measurement techniques and the influence of the oil composition on its detection. Petroleum Science and Technology, 23(9-10), 1113-1128.

Cussler, E.L., Hughes, S.E., and Ward, W.J., Aris, R. (1988) Barrier membrane. Journal of Membrane Science, 38(22), 161-174.

Deen, W.M. (1998) Analysis of Transport Phenomena New York, Oxford University Press.

Dirand, M., Chevallier, V., Provost, E., Bouroukba, M., and Petitjean, D. (1998) Multicomponent paraffin waxes and petroleum solid deposits: Structural and thermodynamic state. Fuel, 77(12), 1253-1260.

Forsythe, W.E. (2003) Smithsonian Physical Tables (9th Revised Edition). Electronic publication, Knovel.

Geankoplis, C.J. (1993) Transport Processes and Unit Operations. New Jersey: Prentice Hall.

González-Salgado, D., Peleteiro, J., Troncoso, J., Carballo, E., and Luís Romaní (2004) Heat capacities, densities and speeds of sound for {(1,5-dichloropentane or 1,6-dichlorohexane) + dodecane} Journal of Chemical and Engineering Data, 49, 333-338.

Guo, X., Pethica, B.A., Huang, J.S., Prud'homme, R.K., Adamson, D.H., and Fetters, L.J. (2004) Crystallization of mixed paraffin from model waxy oils and the influence of micro-crystalline poly(ethylene-butene) random copolymers. Energy and Fuels, 18(4), 930-937.

Hansen, A.B., Larsen, E., Pedersen, W.B., Nielsen, A.B., and Rønningsen, H.P. (1991) Wax precipitation from North Sea crude oils. 3. Precipitation and dissolution of wax studied by differential scanning calorimetry. Energy and Fuels, 5(6), 914-923.

Hammami, A., Ratulowski, J., and Coutinho, J.A.P. (2003) Cloud point: Can we measure or model them? Petroleum Science and Technology, 21(3-4), 345-358.

Haulait-Pirson, M.-C., Huys, G., and Vanstraelen, E. (1987) New predictive equation for the solubility of solid n-Alkanes in organic solvents. Industrial and Engineering Chemistry Research, 26(3), 447-452.

Hayduk, W., and Minhas, B.S. (1982) Correlations for prediction of molecular diffusivities in liquids. Canadian Journal of Chemical Engineering, 60, 295-299.

Hennessy, A.J., Neville, A., and Roberts, K.J. (1999) An examination of additive-mediated wax nucleation in oil pipeline environments. Journal of Crystal Growth, 198-199(PART I), 830-837.

Huyskens, P.L., and Haulait-Pirson, M.C. (1987) A new expression for the combinatorial entropy of mixing in liquid mixtures. Journal of Molecular Liquids, 31(3), 135-151.

Jennings, D.W. and Weispfennig, K. (2005) Effects of shear and temperature on wax deposition: Coldfinger investigation with a Gulf of Mexico crude oil. Energy and Fuels, 19(4), 1376-1386.

Jennings, D.W. and Weispfennig, K. (2006) Effect of shear on the performance of paraffin inhibitors: Coldfinger investigation with Gulf of Mexico crude oils. Energy and Fuels, 20(6), 2457-2464.

Paso, K. G., and Fogler, H.S. (2003) Influence of n-paraffin composition on the aging of wax-oil gel deposits AIChE Journal, 49(12), 3241-3252.

Paso, K., Senra, M., Yi, Y., Sastry, A.M., and Fogler, H.S. (2005) Paraffin polydispersity facilitates mechanical gelation. Industrial and Engineering Chemistry Research, 44(18), 7242-7254.

Schwahn, D., Richter, D., Lin, M., and Fetters, L.J. (2002) Cocrystallization of a poly(ethylene-butene) random copolymer with C24 in n-decane. Macromolecules, 35(9), 3762-3768.

Senra, M. (2006) Assessing the role of polydispersity in n-paraffin solutions. A Preliminary Report for Department of Chemical Engineering University of Michgan Ann Arbor, 1-29.

Senra, M. (2006) Private communication.

Sharma, A., Won, L.D., Buddhi, D., and Park, J.U. (2005) Numerical heat transfer studies of the fatty acids for different heat exchanger materials on the performance of a latent heat storage system. Renewable Energy, 30(14), 2179-2187.

Singh, P. (2000) Gel Deposition on Cold Surfaces. University of Michigan Ph.D. Thesis.

Singh, P., Fogler, H.S., and Nagarajan, N. (1999) Prediction of the wax content of the incipient wax-oil gel in a pipeline: An application of the controlled-stress rheometer. Journal of Rheology, 43 (6), 1437-1459.

Singh, P., Venkatesan, R., Fogler, H.S., and Nagarajan, N. (2000) Formation and aging of incipient thin film wax-oil gels. AIChE Journal, 46(5), 1059-1074.

Singh, P., Venkatesan, R., Fogler, H.S., and Nagarajan, N. (2001) Morphological evolution of thick wax deposits during aging. AIChE Journal, 47(1), 6-18

Srivastava, S.P., Saxena, A.K., Tandon, R.S., and Shekher, V. (1997) Measurement and prediction of solubility of petroleum waxes in organic solvents. Fuel, 76(7), 625-630.

Turner W.R. (1971) Normal alkanes Ind Eng Chem Prod Res Develop, 10(3), 238-260.

Uzomah, T.C. (2000) Prediction of solubilities, the effect of temperature on the solubility of n-alkanes, and the mobile order theory. Journal of Polymer Science, Part A: Polymer Chemistry, 38(1), 43-50.

Venkatesan, R., Nagarajan, N.R., Paso, K., Yi, Y.-B., Sastry, A.M., and Fogler, H.S. (2005) The strength of paraffin gels formed under static and flow conditions. Chemical Engineering Science, 60(13), 3587-3598.

APPENDICES

Appendix A Deposition Simulation

This section will show a deposition simulation created by solving balance equations in chapter 4 numerically to predict wax deposition and to compare with the experimental results.

First, the experimental results of n-alkane fraction in the deposit, as shown in Figure 5.2, will be compared to simulation. To run the monodisperse n-alkane system simulation, C_j and $\dfrac{dC_j}{dT}$ terms are calculated by the modified Flory-Huggins equation, which are shown in Table A.1.

Table A.1 Solubility equations (Huyskens and Haulait-Pirson, 1985)

System	C_j (kg/m³), T (°C)	$\dfrac{dC_j}{dT}$ (kg/m/°K), T (°C)
C_{36}	$0.039 \, e^{\, 0.158T}$	$6.12 \times 10^{-3} \, e^{\, 0.158T}$
C_{32}	$0.139 \, e^{\, 0.153T}$	$2.12 \times 10^{-2} \, e^{\, 0.153T}$
C_{28}	$0.933 \, e^{\, 0.137T}$	$1.28 \times 10^{-1} \, e^{\, 0.137T}$

. The monodisperse deposition predictions in Table A.2 and Figure A.3 were done by using Polymath 5.1 with values from Table A.1 to solve Equations 4.7, 4.9, and 5.2 (See Polymath code in Appendix B).

Table A.2 Deposition numerical results after 6 hours

System	δ (cm)		F_j	
	Model	Experiment	Model	Experiment
C_{36}	0.14	0.14	0.49	0.42
C_{32}	0.1	0.04	0.70	0.26
C_{28}	0.05	0.01	0.89	0.08

The model overpredicts r_i for C_{32} and C_{28} and predicts that higher C_n will have a lower F_j which contradicts the experimental results. Even if α_c in Equation 4.12 was

changed, only one of the trends can be matched because an increase in α causes an increase in r_i, but a decrease in F_j. One important factor that could potentially explain the difference between experimental results and the values from simulation is the shear caused by stirring the system.

Generally, shear from the fluid to the deposit will increase if the flow becomes more turbulent. The turbulence of the system can be estimated by calculating the Reynolds number of this system. The general form of the Reynolds number is

$$\mathrm{Re} = \frac{\rho v_{av} L_{char}}{\mu} \tag{A.1}$$

The characteristic length of the coldfinger is determined by using the diameter of pipe that provides the same cross section area of fluid flow as in the coldfinger system as shown in Figure A.1
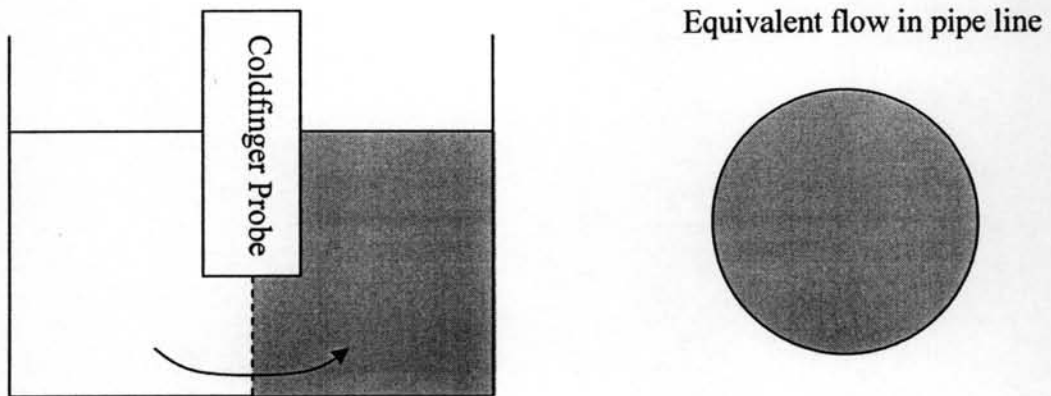

Figure A.1 Equivalent fluid flow cross section area.

The shaded areas represent the equivalent cross section areas of fluid flow in both the coldfinger and the pipe. The values used for calculating the Reynolds number are provided in Table A.3.

Table A.3 Values for calculating Reynolds number

Known parameter	Value	Calculated by
Contact length (L)	2.6 cm	
Liquid height in coldfinger (H)	6.16 cm	
Density of dodecane at 50°C	748 kg/m^3	
Viscosity of dodecane at 50°C	0.911 m Pa·s	
Stirrer rotational frequency	340 rpm	
Cross section area of fluid flow (A$_f$)	18.67 cm^2	
Stirrer rotational radius (r$_s$)	1.89 cm	
Stirrer angular speed (ω)	35.6 rad/s	
Average velocity (v$_{av}$)	0.3356 m/s	$v_{av} = \dfrac{\omega r_s}{2}$
L$_{char}$	4.87 cm	$L_{char} = \left(\dfrac{A_f}{\pi}\right)^{0.5}$

The average velocity is determined by assuming that the coldfinger liquid velocity profile is

$$v = \begin{cases} r\omega; 0 \leq r \leq r_s \\ r_s\omega\dfrac{(R_c - r)}{(R_c - r_s)}; r_s < r \leq R_c \end{cases} \tag{A.2}$$

where r_s is the rotational radius of stir bar and R_c is the coldfinger cylinder radius. From these assumptions, the average velocity at the bottom of the coldfinger is determined to be the velocity at a half length of rotational radius which is one fourth of the stir bar length. By using the parameters discussed in Table A.3, the average velocity at the bottom of the coldfinger, and Equation A.1, the Reynolds number of the system is calculated to be 1.34×10^4. This Reynolds number indicates turbulent flow. Due to the decrease of fluid velocity with the distance from the stir bar, this calculated Reynolds number is higher than the actual Reynolds number in parts of the vessel. However, the system flow would still be turbulent even if the actual

Reynolds number of the system is lowered to a half of this Reynolds number. Thus, fluid in the coldfinger system could provide a significant shear stress affecting deposition characteristic of wax.

Shear from the stir bar could destroy both crystals of soft deposits and crystals that have just nucleated if they are sufficiently weak. If the deposit of lower C_n is weaker than higher C_n, this will strengthen the shear factor argument and help explain why the mathematical model may overpredict more for lower C_n. Another reason supporting this argument is provided in Table A.3.

Table A.4 Monodisperse system maximum r_i and T_i ranges. The range is from using k_w and k_{oil} for k_e

System	δ_{max} range (cm)	δ_{actual} after 6 hours (cm)	T_i (°C)	T_{cloud} (°C)	
				Theory	Experiment
C_{36}	0.19-0.34	0.14	37.8	42.2	40.9
C_{32}	0.09-0.16	0.04	25.2	35.2	33.8
C_{28}	0.03-0.06	0.01	19.7	25.2	23.9

Theoretically, δ will increase until it reaches a maximum when T_i equals the cloud point and the driving force for deposition is zero.

Table A.4 shows that the thickness of the C_{36}, C_{32}, and C_{28} deposits would have to be 36%, 125% and 300% higher respectively in order to reach the thicknesses obtained in the simulation. However, this is unlikely because most of the deposit mass and thickness has already been developed in the first 6 hours as indicated in Figure A.3 and by observation. Moreover, the C_{36} deposit mass does not change after 6 hours as shown in Table 3.5, indicating that the deposit thickness of C_{36} system has reached its maximum.

Shear could be a potential reason to explain why the F_j from simulation deviates from experimental results.
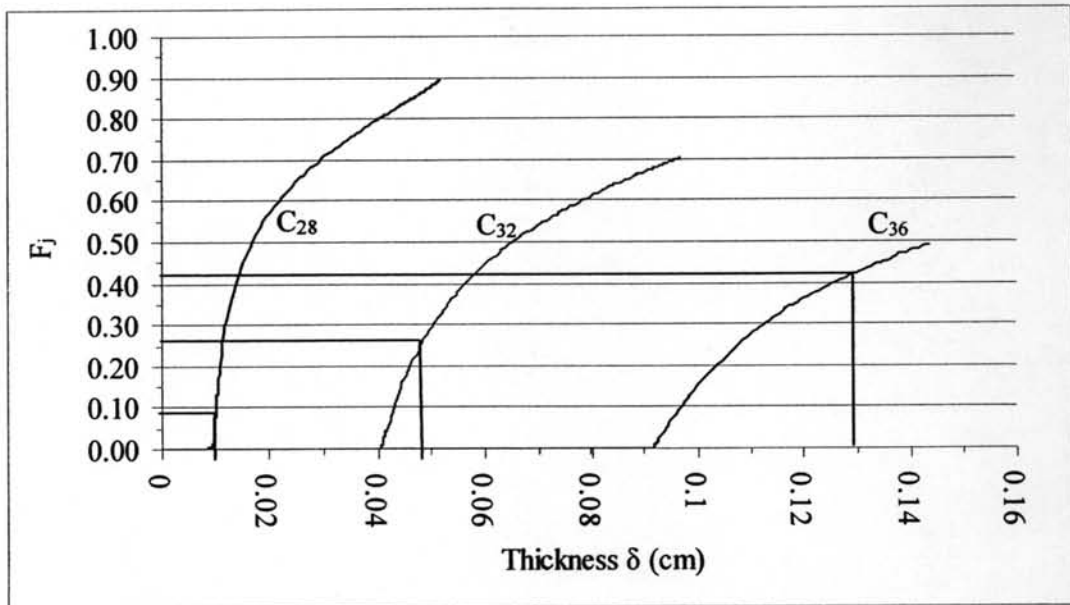
Figure A.2 Predicted F_j as a function of δ. The thick lines represent the actual F_j value and the predicted thickness from the simulation.

Table A.5 Predicted thickness from Figure A.2 using experimental F_j values

System	Actual F_j	δ (cm)	
		Actual	Predicted
C_{36}	0.422 ± 0.036	0.14 ± 0.007	$0.130 \pm 6 \times 10^{-3}$
C_{32}	0.268 ± 0.051	0.04 ± 0.007	$0.049 \pm 2 \times 10^{-3}$
C_{28}	0.800 ± 0.011	0.01 ± 0.007	$0.010 \pm 7 \times 10^{-5}$

By looking at Table A.5, it can be seen that the model could be used to predict the actual wax fraction if we use the actual thickness. For a more accurate prediction of r_i and F_j of wax deposit, a shear reduction term should be added to balance equations. When the shear reduction term is added, the deposit mass and growth balance becomes

Rate of addition	=	Radial convective	-	Diffusive flux	-	Reduction
of species j in		flux of wax molecules		of species j into		rate of species
growing the gel		from the bulk to the		the gel at the		j due to fluid
deposit		fluid-gel interface		deposit interface		shear stress

and

Rate of change of species j in the deposit	=	Radial convective flux of species j molecules form the bulk to the fluid- deposit interface	-	Rate of species j decrease due to fluid shear stress

The shear reduction term is a function of deposit yield stress because weaker deposits are easier to be affected by shear. Thus, further investigation of the deposit yield stress is suggested to perform to gain a better understanding of wax deposition.

The effect of the difference in thermal conductivity between stearic acid and an n-alkane on F_j discussed in section 5.1 is investigated more in this section by using balance equations provided in Chapter 4. The simulation result of balance equation is shown here in Figure A.3 by assuming that stearic acid has the same solubility and diffusivity characteristics as C_{32} but a different thermal conductivity. Figure A.3 comes from solving Equations 4.9, 4.13 and 5.2 numerically and simultaneously by using Polymath 5.1, an ODE solver. The solubility of C_{32} is calculated from the modified Flory-Huggins equation.
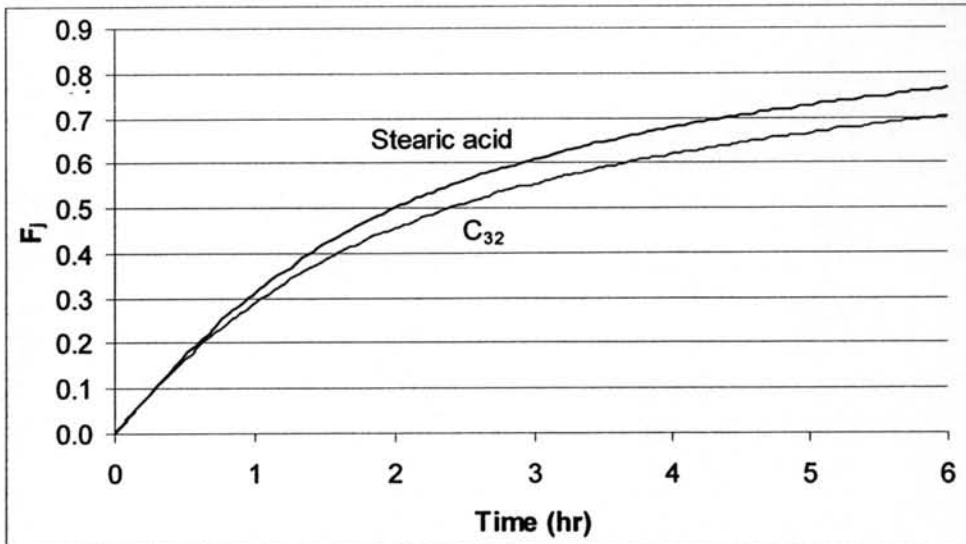
Figure A.3 Prediction of F_j of stearic acid and C_{32} as a function of time.

Figure A.3 shows that the decrease in thermal conductivity of stearic acid from C_{32} by 31% increases F_j from 0.7 to 0.76, about 10%. However, the experimental result in Figure 5.2 shows that F_{Str} is about double F_{C32}. Therefore, other factors must also explain why F_{Str} is higher than F_{C32}. Equation 4.13 suggests that the difference could be explained by the effective diffusivity of stearic acid, because if D_{ej} increases, F_j will also increase.

Appendix B Notations

α = average aspect ratio of crystals in deposit

δ = deposit thickness (cm)

δ_{actual} = actual deposit thickness from the experiment (cm)

δ_{max} = maximum deposit thickness (cm)

$$\vec{\nabla} = \frac{\partial}{\partial r}\hat{r} + \frac{1}{r}\frac{\partial}{\partial \theta}\hat{\theta} + \frac{\partial}{\partial z}\hat{z}$$

μ = viscosity (Pa·s)

ρ = density (kg/m^3)

ρ_{gel} = deposit density (kg/m^3)

ω = stirrer rotational speed (rad/s)

A = coldfinger probe-deposit contact area (m^2)

A_f = cross section are of fluid flow (m^2)

C_{jb} = liquid phase concentration of species j in bulk (kg/m^3)

C_j = liquid phase concentration of species j (kg/m^3)

C_{ji} = liquid phase concentration of species j at deposit interface (kg/m^3)

C_w = liquid phase concentration of all depositable material (kg/m^3)

C_p = specific heat capacity (J/kg/K)

D_{ej} = effective diffusivity of species j in the deposit (m^2/s)

D_{jo} = diffusivity of species j in oil which is dodecane (m^2/s)

F_j = fraction of species j in the deposit

F_w = fraction of all depositable material in the deposit

h = convective heat transfer coefficient (W/m^2/K)

H = liquid height in coldfinger (m)

ΔH_j = heat of solidification of species j (J/mol)

k_{C12} = thermal conductivity of dodecane (W/m/K)

k_e = effective thermal conductivity of the deposit (W/m/K)

k_{lj} = the mass transfer coefficient of species j in liquid l (m/s)

k_{oil} = thermal conductivity of oil (W/m/K)

k_w = wax thermal conductivity (W/m/K)

L = deposit height (m)

L_{Char} = system characteristic length (m)

m_j = mass of species j in the deposit (kg)

q = conduction heat through the deposit (W)

r_i = radius of deposit interface (m)

r_s = rotational radius of stir bar (m)

R = coldfinger probe radius (m)

R_c = coldfinger cylinder radius (m)

t = time (sec)

T = temperature (°C)

T_a = coldfinger temperature (°C)

T_b = bulk temperature (°C)

T_{b0} = initial bulk temperature (°C)

T_{cloud} = cloud point temperature (°C)

T_i = fluid-deposit interface temperature (°C)

U = equivalent velocity of coldfinger system for flow loop (m/s)

V = volume of liquid in coldfinger (m^3)

v = velocity of fluid in coldfinger (m/s)

v_{av} = average velocity of fluid in coldfinger (m/s)

V_g = volume of the deposit (kg/m^3)

Nu = Nusselt number ($\dfrac{hL_{char}}{k_{oil}}$)

Re = Reynolds number ($\dfrac{\rho v_{av} L_{char}}{\mu}$)

Sc = Schmidt number ($\dfrac{k_{lj} L_{char}}{D_{jo}}$)

Appendix C Numerical Method Code

POLYMATH Results
No Title   03-11-2007, Rev5.1.233

Calculated values of the DEQ variables

Variable	initial value	minimal value	maximal value	final value
t	0	0	2.16E+04	2.16E+04
Fi	1.0E-09	1.0E-09	0.4921999	0.4921999
ri	0.0047	0.0047	0.0061365	0.0061365
Kw	0.25	0.25	0.25	0.25
KC12	0.1317	0.1317	0.1317	0.1317
alpha_con	1	1	1	1
T0	318.92448	318.92448	318.92448	318.92448
B	631.20424	631.20424	631.20424	631.20424
Ta	10	10	10	10
Tb	50	50	50	50
ke	0.1317	0.1317	0.1763498	0.1763498
alpha	1	1	1.4921999	1.4921999
Dio	7.071E-10	7.071E-10	7.071E-10	7.071E-10
rhoC12	748	748	748	748
hi	235.1	235.1	235.1	235.1
R	0.0047	0.0047	0.0047	0.0047
Ti	10.000714	10.000714	37.428279	37.428279
Ci	0.1877862	0.1877862	14.164851	14.164851
dCi_dT	0.0295991	0.0295991	2.2326822	2.2326822
dT_dr_i	7.14E+04	1.676E+04	7.14E+04	1.676E+04
dCi_dr	2113.4773	2113.4773	4.27E+04	3.742E+04
kl	1.262E-06	1.262E-06	1.262E-06	1.262E-06
Cib	29.9	29.9	29.9	29.9
Va	621.3	621.3	621.3	621.3
mu	1.7784893	1.1302807	1.7784893	1.1302807
Djo	3.559E-10	3.559E-10	5.793E-10	5.793E-10
Dei	3.559E-10	2.809E-10	5.622E-10	2.809E-10

ODE Report (RKF45)

Differential equations as entered by the user
[1] d(Fi)/d(t) = 2*ri*Dei*dCi_dr/(rhoC12*(ri*ri-R*R))
[2] d(ri)/d(t) = (kl*(Cib-Ci)-Dei*dCi_dr)/(Fi*rhoC12)

Explicit equations as entered by the user
[1] Kw = 0.25
[2] KC12 = 0.1317
[3] alpha_constant = 1
[4] T0 = 318.92448
[5] B = 631.20424
[6] Ta = 10
[7] Tb = 50
[8] ke = (2*Kw+KC12+(Kw-KC12)*Fi)/(2*Kw+KC12-2*(Kw-KC12)*Fi)*KC12
[9] alpha = 1+alpha_constant*Fi
[10] Dio = 0.707095*(10^(-9))
[11] rhoC12 = 748
[12] hi = 235.1
[13] R = 0.0047
[14] Ti = (ri*hi*Tb*ln(ri/R)+ke*Ta)/(ke+ri*hi*ln(ri/R))
[15] Ci = 0.038821*exp(0.157623*Ti)
[16] dCi_dT = 0.1576213*Ci
[17] dT_dr_i = (Ti-Ta)/(ri*ln(ri/R))
[18] dCi_dr = dCi_dT*dT_dr_i

[19] kl = hi*Dio/KC12
[20] Cib = 29.9
[21] Va = 621.3
[22] mu = 10^(B*(1/(Ti+273.15)-1/T0))
[23] Djo = 10^(-4)*13.3*10^(-8)*(Ti+273.15)^1.47*mu^(10.2/Va-0.791)*Va^(-0.71)
[24] Dei = Djo/(1+(alpha^2)*(Fi^2)/(1-Fi))

Comments

[1] d(Fi)/d(t) = 2*ri*Dei*dCi_dr/(rhoC12*(ri*ri-R*R))   *Average fraction of species i of the deposit*
    1/sec F from experiment after 6 hours is 0.4217
[2] d(ri)/d(t) = (kl*(Cib-Ci)-Dei*dCi_dr)/(Fi*rhoC12)   *m/s ri from experiment 6hr = 0.61 cm*
[3] Ti =   (ri*hi*Tb*ln(ri/R)+ke*Ta)/(ke+ri*hi*ln(ri/R))   *'C*
[4] ke =   (2*Kw+KC12+(Kw-KC12)*Fi)/(2*Kw+KC12-2*(Kw-KC12)*Fi)*KC12   *W/m/ 'K*
[5] alpha =   1+alpha_constant*Fi   *assume that aspect ratio change with Fw linearly*
[6] Dei = Djo/(1+(alpha^2)*(Fi^2)/(1-Fi))   *effective diffusivity of wax inside the gel (m^2/s)*
[7] Djo = 10^(-4)*13.3*10^(-8)*(Ti+273.15)^1.47*mu^(10.2/Va-0.791)*Va^(-0.71)
    From Perry, Singh et al 2000, Hayduk and Minhas 1982 (m2/s)
[8] Ci = 0.038821*exp(0.157623*Ti)   *Kg/m^3 for C36 from Haulait-Pirson, M.C. 1987*
[11] alpha_constant = 1   *first guess*
[12] Dio = 0.707095*(10^(-9))   *m2/s for C36 at 50C using for estimate klj*
[13] rhoC12 =   748   *Kg/m3*
[14] hi =   235.1   *W/m^2/ 'K*
[15] R =   0.0047   *m: coldfinger radius*
[16] Tb =   50   *'C*
[17] Ta =   10   *'C*
[18] Kw =   0.25   *W/m/ 'K Typical value*
[19] KC12 =   0.1317   *W/m/ 'K @ 323.15 'K at 298.15 is 0.1360*
[21] kl =   hi*Dio/KC12   *mass transfer coefficient of system (m/s)*
[22] Cib =   29.9   *kg/m3 assume that C of bulk fluid is constant*
[23] Va =   621.3   *cm3/mol For C36*
[24] mu = 10^(B*(1/(Ti+273.15)-1/T0))   *mu (m Pa s) using relation from Perry 7th edition*
    page 2-365 - 2-366
[25] B = 631.20424   *B for calculate mu*
[26] T0 = 318.92448   *K for calculate mu*

Independent variable
 variable name : t
 initial value : 0
 final value : 21600

Precision
 Step size guess. h = 0.000001
 Truncation error tolerance. eps = 0.000001

General
 number of differential equations: 2
 number of explicit equations: 24
 Data file: C:\Ko\BMSDATA\simulation FW\theory C36 in 4C36C12 Fw sim.pol

CURRICULUM VITAE

Name: Mr. Ekarit Panacharoensawad

Date of Birth: April 22, 1983

Nationality: Thai

University Education:

    2001-2005 Bachelor's Degree of Physics (First Class Honors), Faculty of Science, Chulalongkorn University, Bangkok, Thailand

Conference:

    2006   Biannual meetings of the Porous Media Research Group

           (Attendees include: Chevron, ConocoPhillips, Nalco,

           Schlumberger, Shell, Total) 3rd June, Ann Arbor, Michigan